JOURNAL OF SOLID STATE CHEMISTRY **140,** 295–299 (1998)
ARTICLE NO. SC987890

Emf Measurements on Nanocrystalline Copper-Doped Ceria

P. Knauth,* G. Schwitzgebel,† A. Tschöpe,‡ and S. Villain*

*Laboratoire de Métallurgie EDIFIS (UMR CNRS 6518), Faculté des Sciences de Marseille-St Jérôme, Case 511, 13397 Marseille Cedex 20, France; and †FR Physikalische Chemie, and ‡FR Technische Physik, Universität des Saarlandes, 66041 Saarbrücken, Germany

Received February 2, 1998; in revised form May 12, 1998; accepted May 19, 1998

Mixed oxide samples of nanostructured $Cu_xCe_{1-x}O_{2-y}$ of various composition were generated by (i) chemical precipitation and ball milling and (ii) inert gas condensation. X-ray diffraction measurements suggested that copper oxide was dissolved in nanostructured cerium oxide up to concentrations of $x = 0.15$. Solid electrolyte cells of the type A, $Cu_2O/CuBr/Cu_xCe_{1-x}O_{2-y}$ (A = Cu or CuO) showed reversible cell voltages. The ratio of the formal chemical activities of CuO and Cu_2O dissolved in nanostructured cerium oxide were calculated from the cell voltages. The results are discussed in terms of an apparent macroscopic solubility, due to interfacial segregation of copper oxide on nanostructured cerium oxide. © 1998 Academic Press

INTRODUCTION

The thermodynamic activity, which is defined for solutes in solutions, increases monotonically with the concentration of the solute. In systems with positive enthalpy of mixing, the activity may rise rapidly until the equilibrium solubility is reached, and then the solute precipitates as a new phase. An apparent enhanced macroscopic solubility of a component can be observed in materials with special microstructure. More often, the total solubility is increased in materials with high specific grain boundary area (1), due to grain boundary segregation. The same observation can be made for surface segregation, and the latter case is of particular interest in catalysis. Catalytic activity and selectivity of a catalyst depend on the details of the surface chemistry which can only roughly be estimated from volume phase equilibrium data.

The aim of the present study is to determine the "formal thermodynamic activities" of copper oxides in mixed nanostructured copper–cerium oxide. The term "formal" means that a thermodynamic quantity, which is defined for a homogeneous phase, is used for a non-homogeneous material. Mixed copper–cerium oxide has recently been investigated for catalytic activity in SO_2 reduction by CO (2, 3) and in CO oxidation (3, 4). It was found that these base metal catalysts exhibit activities comparable to precious metal catalysts. The catalytic activity of the mixed oxide was also higher than that of unsupported pure copper or cerium oxide pointing to an important support interaction. Microstructural analysis of a $Cu_{0.15}Ce_{0.85}O_y$ sample by X-ray diffraction (XRD) (5) and scanning transmission electron microscopy (STEM) (6) revealed that copper oxide was highly dispersed on cerium oxide and that this dispersion was remarkably stable up to 923 K. CuO began to form as a distinct phase during annealing at temperatures above 823 K. This coincided with the grain growth of the cerium oxide matrix. The question arises of whether this decrease in the apparent macroscopic solubility corresponds to a decrease of bulk solubility or whether it is a mere consequence of the loss of interfacial area, so that CuO is forced to crystallize, for which the thermal activation is likely sufficient.

To our knowledge, no phase diagram of the Cu–Ce–O system has been established to date. However, the solubility of copper in the CeO_2–fluorite lattice must be expected to be low due to the difference in ionic radii. Electron paramagnetic resonance studies (7) showed that CeO_2 containing 1% Cu exhibited surface segregation with an enrichment factor of 25, which supports the assumption of a rather low solubility in the CeO_2 structure. In the related Cu–Zr–system (8) no ternary compound and a very small solid solubility of copper in the cubic ZrO_2 modification have been reported.

Potentiometric measurements seemed well adapted to measure the Cu activity in nanocrystalline ceria, because the emf of an electrochemical cell depends on the thermodynamic activity of the components in the electrodes. A suitable electrochemical cell can be built up when the reversible potentials can be measured, i.e., when the interesting component in the nanostructured material takes part in the local electrochemical equilibrium. As electrolyte, we chose copper(I) bromide, which is a solid Cu^+-ion conductor. Its conductivity is predominantly ionic above 200°C. At 400°C, the electronic transference number is only 2×10^{-5} and the total conductivity is about 1 S cm^{-1} (9). The cell works at moderately elevated temperatures, where the microstructure of the nanostructured material remains metastable and grain growth is still negligible, but exchange current

0022-4596/98 $25.00

densities are high enough to permit the measurement of reversible potentials.

EXPERIMENTAL

Nanocrystalline Cu-doped cerium oxide samples were prepared by two different techniques: ball milling of precipitated cerium oxide after addition of copper(I) oxide powder (i) and inert gas condensation of Cu–Ce nanoclusters by sputtering of a mixed Cu–Ce target and subsequent *in situ* oxidation (ii).

(i) Cerium carbonate was precipitated from aqueous solutions of cerium nitrate (0.2 M) and ammonium carbonate (0.35 M). The precipitate was filtered and washed twice with deionized water, dried at 353 K, and calcined at 813 K for 5 h in air. The cerium oxide was mixed with the proper amounts of commercial microcrystalline Cu_2O (Chempur), and the mixture was milled for 10 h in a SPEX 2000 ball mill equipped with ZrO_2 vial and balls. The mixed oxide powder was annealed for 5 h in air at 473 K and then for 2 h in vacuum at 473 K. In this paper, the various sample compositions are represented by the Cu cation fraction x, i.e. $Cu_xCe_{1-x}O_{2-y}$. The mixed oxide powders were pressed into porous, self-supporting pellets by uniaxial room temperature compaction at a pressure of 700 MPa.

(ii) In the second preparation route, $Cu_{0.15}Ce_{0.85}O_{2-x}$ was synthesized by magnetron sputtering and inert gas condensation. A mixed metal target of $Cu_{15}Ce_{85}$ composition was sputtered at 20 Pa argon pressure. Due to this pressure, nanoclusters were formed in the gas phase and collected on a cold substrate. After sputtering, the metallic nanoclusters were oxidized by slowly backfilling the vacuum chamber with oxygen. Further details on the synthesis are given elsewhere (5).

X-ray diffraction (XRD) of the samples was performed using a Siemens D500 diffractometer, equipped with primary monochromator and position-sensitive detector (M Braun). Peak profiles of the (111) and (222) reflections were corrected for instrument line broadening, and the volume-weighted mean column length $\langle L \rangle_{vol}$, which serves as a measure for grain size, was determined by the Kochendorfer analysis.

Electrochemical measurements were performed at 593 K in one-compartment cells under a static atmosphere of pure argon. Reference electrodes and solid electrolyte pellets were prepared by compression of pure powders (CuBr, 99.999%, Johnson-Matthey; Cu_2O, CuO, 99%) under 700 MPa. To eliminate transient defects due to compression, the pellets were annealed during several hours at 593 K. The cells were built up by pressing the pellets against one another using thin foils of Cu for the Cu/Cu_2O and Pt for the Cu_2O/CuO as electronic contacts between the electrolyte and the electrode materials. Thus, the sites where the electrical potential forms are not in a direct connection with the gas atmosphere (10), i.e., the electrodes can be considered as closed, especially in the case of Cu halides which have a certain ductility at higher temperatures. A high impedance electrometer was used for emf measurements (Keithley 617); reversibility tests were performed with a high precision constant current source (Keithley 220).

RESULTS

X-Ray Diffraction

The XRD profiles of a $Cu_{0.1}Ce_{0.9}O_{2-y}$ sample before and after ball milling (Fig. 1) showed broad diffraction peaks of the CeO_2–fluorite lattice. Analysis of the peak broadening yielded a column length $\langle L \rangle_{vol}$ of 18 nm. In addition to the CeO_2 peaks, sharp lines attributed to microcrystalline Cu_2O were observed in the diffraction pattern before ball milling. These lines were completely absent after ball milling, indicating the dissolution of the Cu_2O phase in the nanostructured CeO_2.

Samples with x higher than 0.15 showed XRD peaks due to pure copper(I) oxide even after ball milling (6). This confirms that the limit of the apparent solubility of copper oxide in nanocrystalline cerium oxide was reached near this concentration.

Emf Measurements

For a control, the emf of cell [1] was measured between 573 and 623 K.

$$\text{Cell [1]: } (-)\ \text{Cu, } Cu_2O \,|\, \text{CuBr} \,|\, \text{CuO, } Cu_2O\ (+)$$

In Fig. 2 the results are compared with values obtained from thermodynamic tables (11, 12) for the Gibbs free energy function ΔG_T° of the cell reaction

$$Cu + CuO \rightarrow Cu_2O. \qquad [1]$$

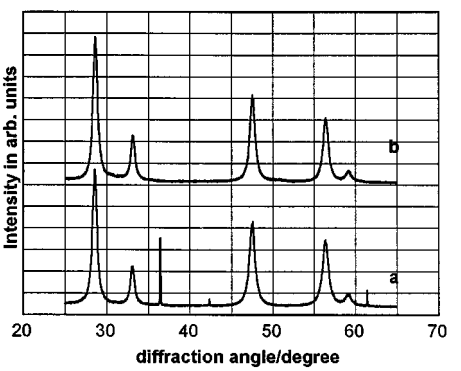

FIG. 1. XRD profiles (Cu$K\alpha$ radiation) of a $Cu_{0.1}Ce_{0.9}O_{2-y}$ sample (a) before and after (b) ball milling.

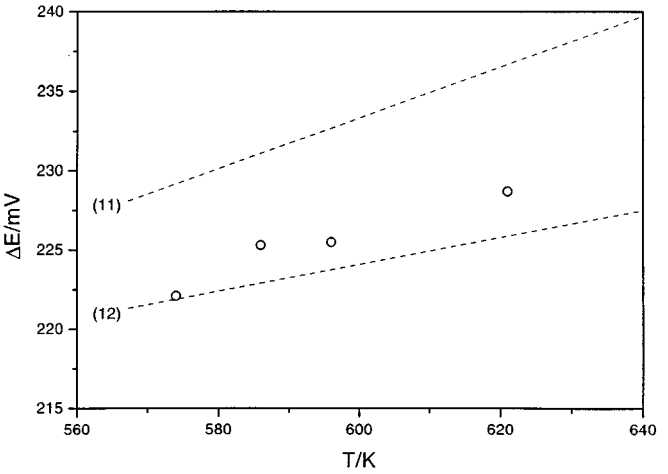

FIG. 2. Emf of cell [1]: Cu, Cu_2O | CuBr | CuO, Cu_2O.

For the investigation of the nanostructured samples, different cells were built up using either side of cell [1] as reference electrodes, which therefore differ by their copper and oxygen activities.

$$\text{Cell [2]: } (-)\ \text{Cu, } Cu_2O/CuBr/Cu_xCe_{1-x}O_{2-y}\ (+)$$

$$\text{Cell [3]: } (-)\ Cu_xCe_{1-x}O_{2-y}/CuBr/Cu_2O,\ CuO\ (+)$$

The cell voltages stabilized rapidly (Fig. 3), and the results for various cation fractions x of the nanostructured $Cu_xCe_{1-x}O_{2-y}$ samples, measured at 593 K, are reported in Table 1.

DISCUSSION

The electrode reactions of cell [1] are

$$(-)\quad Cu \rightarrow Cu^+ + e^- \text{ (oxidation)}, \qquad [2]$$

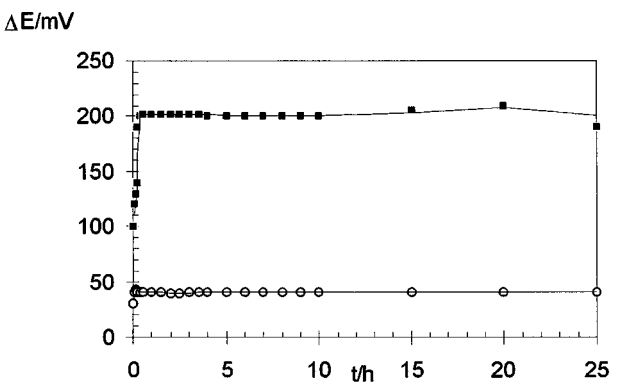

FIG. 3. Time dependency of emf for typical experiments at 593 K. $Cu_{0.1}Ce_{0.9}O_{2-y}$: (■) cell [2]; (○) cell [3].

TABLE 1

Emf Values, $\Delta E(2)$, $\Delta E(3)$, of Cells [2] and [3] for Different $Cu_xCe_{1-x}O_y$ Samples ($T = 593$ K, Samples Prepared by Ball Milling; Exception i.c., Inert Gas Condensation)

x %	$\Delta E(2)$/mV	$\Delta E(3)$/mV
0.25	107	116
0.45	148	90
1 (i.c.)		105
5		81
10	200	40
10		72
15 (i.c.)		55
15		20
20	220	15
25		15
30	220	15

and

$$(+)\quad Cu^+ + e^- + CuO \rightarrow Cu_2O \text{ (reduction)}, \qquad [3]$$

leading to the cell reaction of Eq. [1]. As the two copper oxides are present in pure form, we measure the standard emf, and the related thermodynamic quantity is the standard Gibbs free energy of reaction [1] (F: Faraday constant). The electrodes compartments were not separated; however, the slow oxygen transport through the gas phase from the CuO/Cu_2O to the Cu_2O/Cu reference electrode does not interfere with the electrode equilibrium, as long as the materials involved in the electrode reaction are not altered. Therefore, our cells with halide electrolytes are not influenced when special electrode setups are used (see Experimental section).

$$\Delta E^\circ = -\Delta G^\circ_T/F. \qquad [4]$$

The results (Fig. 2) are probably the most reliable values for ΔE° or ΔG° in this T region, because other values have to be calculated either by extrapolation from more than 200 K higher temperatures or by using standard data of insufficient precision (11, 12).

For cell [2], the electrode reaction at the negative pole is the same as in cell [1], i.e., Eq. [2], but at the positive pole CuO (ns) distributed in the nanostructured material is transformed to Cu_2O (ns), also in the nanostructured state (ns).

$$(+)\quad CuO_{ns} + Cu^+ + e^- \rightarrow Cu_2O_{ns}. \qquad [5]$$

The cell reaction is thus the same as in cell [1] with the important difference that both oxides are no longer present in the standard state but dispersed in cerium oxide. The activity ratio r of CuO_{ns} and Cu_2O_{ns} may be written as

a function of the cell voltage using the standard emf ΔE° and measured ΔE [2] of cell [2].

$$r = a(CuO_{ns})/a(Cu_2O_{ns}) = \exp[(\Delta E[2] - \Delta E^\circ)F/(RT)]. \quad [6]$$

For cell [3], the electrode reaction of the negative pole is

$$(-) \quad Cu_2O_{ns} \rightarrow CuO_{ns} + e^- + Cu^+. \quad [7]$$

When combined with Eq. [3], the cell reaction

$$Cu_2O_{ns} + CuO \rightarrow CuO_{ns} + Cu_2O \quad [8]$$

results, which is an exchange reaction of copper oxides between the nanostructured and the pure reference state. The activity ratio is given by ΔE [3] of cell [3]:

$$r = a(CuO_{ns})/a(Cu_2O_{ns}) = \exp(-F\Delta E[3]/RT). \quad [9]$$

In some cases (cf. Table 1), samples with the same molar fractions x were studied in cell [2] and cell [3]. According to Eqs. [6] and [9], the sum of their emf's should be equal to ΔE°. In the case of experiments with x equal 0.20, 0.25, and 0.30, where excess Cu_2O was found by XRD, the emf of cell [3] is 15 mV and that of cell [2] is by 5 mV below ΔE° from cell [1]. This means the electrode components are in the state of nanocrystallinity, but Eqs. [6] and [9] would lead to different results for r. This discrepancy may also be a consequence of the different O_2 partial pressures in cell [2] and cell [3], the stoichiometry of nanocrystalline oxides being sensibly dependent on the oxygen pressure. This asymmetry of the $Cu_xCe_{1-x}O_{2-y}$ electrodes in cell [2] and cell [3] can be eliminated by using $\Delta E^\circ_{calc} = 235$ mV in Eq. [6], which was done for r in Fig. 4.

With the mean value of $\Delta E_{ex} = 10$ mV, supposed to be due to nanocrystallinity of the electrode material, the interfacial excess free energy $|\Delta G_{ex}| = F\Delta E_{ex}$, can be interpreted according to a general equation [10] which is related to the mean particle diameter d (13).

$$\Delta G_{ex} = 2g\tau V/d \quad [10]$$

(τ, specific interfacial free energy; V, molar volume; g, geometrical factor (near 1)).

With $d = 18$ nm and $V = 24\ cm^3\ mol^{-1}$ (the value of CeO_2, on which the copper oxide is adsorbed), one obtains an usual value for $\tau = 0.3\ J\ m^{-2}$.

Figure 4 shows the activity ratio r as a function of the copper content x of the samples. When leaving out of account the values obtained for the inert gas samples (cf. Table 1), the curve obviously exhibits special features. A tentative explanation of the curve can be given with the assumption that copper oxide segregates on CeO_{2ns} in layers. With a mean grain diameter of about 18 nm, one needs approximately a molar fraction $x \approx 0.1$ to form a monolayer of Cu and O atoms at the grain interfaces, and the curve up to this x value, probably corresponding to the formation of this monolayer, can be represented by a modified Langmuir–MacLean equation, Eq. [11]:

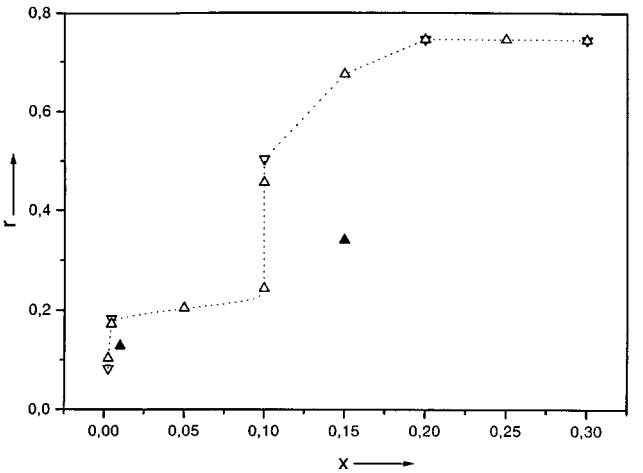

FIG. 4. Ratio r of the thermodynamic activities $a(CuO_{ns})/a(Cu_2O_{ns})$ in nanostructured $Cu_xCe_{1-x}O_{2-y}$: (▽) cell [2]; (△) cell [3]; (▲) i.c. sample in cell [3].

$$r = x\exp(\Delta G_{seg}/RT)/[1 + x\exp(\Delta G_{seg}/RT)]. \quad [11]$$

The free energy of segregation, $\Delta G_{seg} \approx 0.4$ eV, which is related to the misfit strain energy resulting from differences of the radii of the host (Ce^{4+}) and dopant ions (Cu^+ or Cu^{2+}) matches with a copper radius between that of Cu^+ and Cu^{2+} (14). The further trace of the curve even seems to indicate the building of the second layer, until Cu_2O appears as a new phase marked by the plateau ($x > 0.15$) and confirmed by the X-ray results. The r values of the inert gas samples correspond to a lower grain diameter of the material, so that the layer formation is shifted to higher x values.

ACKNOWLEDGMENTS

The support of the Deutsche Forschungsgemeinschaft within the frame of SFB 277 is gratefully acknowledged. S.V. expresses thanks for guest scholarship in the SFB.

REFERENCES

1. R. Birringer, H. Hahn, H. Höfler, J. Karch, and H. Gleiter, *Defect Diffusion Forum* **59,** 17 (1988).
2. W. Liu, A. F. Sarofim, and M. Flytzani-Stephanopoulos, *Appl. Catal. B* **4,** 167 (1994).
3. A. Tschöpe W. Liu, M. Flytzani-Stephanopoulos, and J. Y. Ying, *J. Catal.* **157,** 42 (1995).

4. W. Liu and M. Flytzani-Stephanopoulos, *J. Catal.* **153,** 304 (1995).
5. A. Tschöpe and J. Y. Ying, *Nanostruct. Mater.* **4,** 617 (1994).
6. A. Tschöpe, J. Y. Ying, and Y.-M. Chiang, *Mater. Sci. Eng. A* **204,** 267 (1995).
7. A. Aboukais, A. Bennani, C. F. Aissi, G. Wrobel, M. Guelton, and J. C. Vedrine, *J. Chem. Soc., Faraday Trans.* **88,** 615 (1992).
8. E. M. Levin, C. R. Robbins, and H. F. McMurdie, "Phase Diagrams for Ceramists" M. K. Reser, Ed.), Suppl. Vol. 3. The American Ceramics Society, Columbus, OH, 1996.
9. S. Villain, M.-A. Desvals, G. Clugnet, and P. Knauth, *Solid State Ionics* **83,** 191 (1991).
10. G. Schwitzgebel, G. Flohr, and S. Zorner, *J. Chem. Thermodynamics*, **18,** 247 (1986).
11. O. Kubaschewski and C. B. Alcock, "Metallurgical Thermochemistry." Pergamon Press, Oxford, 1979.
12. D. L. Lide, Ed., "Handbook of Chemistry and Physiocs." CRC Press, Boca Raton, FL, 1997.
13. L. E. Chen and F. Spaepen, *J. Appl. Phys.* **69,** 689 (1991).
14. D. A. Blom and Y. M. Chiang, Aliovalent Grain Boundary Segregation in Heavily Doped Ceria, *in* "US–Japan Workshop on Electrically Active Ceramic Interfaces" (H. Yanagida and H. L. Tuller, Eds.). Cambridge, MA, 1998.